JOURNAL OF SPACECRAFT AND ROCKETS
Vol. 29, No. 1, January–February 1992

Land-Mobile-Satellite Fade Measurements in Australia

Wolfhard J. Vogel*
University of Texas at Austin, Austin, Texas 78758
Julius Goldhirsh†
Applied Physics Laboratory, Johns Hopkins University, Laurel, Maryland 20707
and
Yoshihiro Hase‡
Communications Research Center, Tokyo, 184, Japan

Attenuation measurements were implemented at L-band (1.5 GHz) in southeastern Australia during an 11-day period in October 1988 as part of a continuing examination of the propagation effects due to roadside trees and terrain for mobile-satellite service. Beacon transmissions from the geostationary ETS-V and IPORS satellites were observed. The Australian campaign expanded to another continent our Mobile Satellite Service data base of measurements executed in the eastern and southwestern United States regions. An empirical fade distribution model based on U.S. data predicted the Australian results with errors generally less than 1 dB in the 1–20% probability region. Directive antennas are shown to suffer deeper fades under severe shadowing conditions (3 dB excess at 4%), the equal-probability isolation between co- and cross-polarized transmissions deteriorated to 10 dB at the 5 dB fade level, and antenna diversity reception may reduce unavailability of the system by a factor of 2–8.

Nomenclature

d = antenna separation, m
F = fade depth exceeded, dB
P = percentage of distance travelled, %
P_0 = single antenna probability distribution
P_d = dual antenna probability distribution
Θ = elevation angle, deg

Introduction

MOBILE satellite systems are expected to provide telephone and data communications to private, commercial, and government vehicles, especially in rural, low-population-density areas where terrestrial cellular services are unavailable. In designing these future mobile satellite systems, communication engineers require information on fade statistics associated with shadowing and multipath propagation due to roadside obstacles and terrain.

To obtain data of this type, the authors previously[1-7] employed transmitter platforms, such as stratospheric balloons, remotely piloted aircraft, helicopters, and the INMARSAT B2 geostationary satellite, at ground locations in the eastern and southwestern U.S. regions. The objectives of the earlier measurement campaigns were to assess the statistics of fades under the following variable conditions: roadside obstacles, mountainous and flat terrain, elevation angles, side of roads and directions driven, seasonal effects, and unshadowed vs shadowed line-of-sight conditions.

The Australian campaign offered the opportunity to determine fade statistics for a continent having different types of foliage and terrain. It also enabled a broadening of a limited fade data base involving satellite platforms.[5,8,9] Measurements of transmissions radiated from the Experimental Technology Satellite (ETS-V) were predominantly accessed, although signals emanating from the Pacific Ocean Region Satellite (IPORS) were also received over a significant number of runs. Unlike the previous tests, the Australian experiment enabled the following: 1) high- and low-gain antennas were used over repeated runs, 2) transmissions from two different satellites allowed probing fade variability with different azimuthal and elevation directions, and 3) cross-polarization signal levels were measured during selected runs.

In this effort we present fade statistics based on data selected from the campaign total of 1436 km of roads sampled. The culled data set corresponds to 460 km of roads and encompasses 36 runs, a run representing a particular stretch of road with consistent parameters over which measurements were obtained and cataloged. Results pertaining to the following are exhibited: 1) fade distributions for different road types and differing densities of roadside obstacles (trees and utility poles), 2) overall average fade distribution and comparison with a previously derived empirical model, 3) distributions for opposite directions of driving, 4) fade distributions for different mobile antenna patterns (high-gain vs low-gain), 5) fade distributions for different satellite transmitter platforms, 6) cross-polarization fade statistics, and 7) simulated diversity gain improvement. Statistics associated with urban driving are not discussed, as terrestrial cellular systems are expected to be available at such locations.

Experimental Aspects

Transmitter and Antenna Systems

The experimental parameters are summarized in Table 1. Left-hand circularly polarized (LHCP) beacon transmissions from ETS-V, radiated with an effective integrated radiated power (EIRP) of 25.9 dBW, were received at a frequency of 1545.15 MHz. Elevation angles ranged from 51 deg in Sydney to 56 deg in Coolangatta; the azimuth was −2 deg. Although most of the selected measurements are for this satellite (28 runs, 446 km), measurements from IPORS (EIRP of 20 dBW) are also included for a significant number of runs (10 runs, 68 km). These right-hand circularly polarized (RHCP) transmissions were received at a frequency of 1541.5 MHz, elevation of 40 deg, and azimuth of 45 deg in Sydney.

Received July 30, 1990; revision received Jan. 4, 1991; accepted for publication Jan. 5, 1991.

*Electrical Engineering Research Laboratory, 10100 Burnet Road. Member AIAA.
†Johns Hopkins Road.
‡Communications Research Laboratory, Ministry of Posts and Telecommunications, 4-2-1, Nukui-kita, Koganei.

Table 1 Summary of salient transmitter and receiver system parameters

	Satellite	
	ETS-V	IPORS
Azimuth at Sydney	−2 deg	45 deg
Elevation at Sydney	51 deg	40 deg
Frequency	1545.15 MHz	1541.5 MHz
EIRP	25.9 dBW	20 dBW
Polarization	LHCP	RHCP
SNR low-gain copolarized	22.4 dB	16.4 dB
SNR high-gain copolarized	32.4 dB	—
Receiver bandwidths	500 Hz (quad. detectors) 200 Hz (filter)	
Sampling rate	1 kHz	
Data recorded	Quadrature detector outputs 200 Hz filter output Vehicle speed Time	
Receiver antenna	Low-gain crossed drooping dipole	High-gain helix
Gain	4 dB	14 dB
Elevation pattern	15 to 70 deg	45 deg (3 dB)
Azimuth pattern	omni	45 deg (3 dB)
Polarization (ETS-V)	LHCP	LHCP, RHCP
Polarization isolation	—	>20 dB
Polarization (IPORS)	RHCP	—

The low-gain receiving antennas (RHCP and LHCP) were crossed drooping dipoles with 4-dB gain, azimuthally omnidirectional radiation patterns, and elevation patterns that were relatively flat over the 15 to 75 deg interval. They were mounted one at a time on the roof of the mobile unit 2 m above ground and with fixed vertical pointing. The high-gain antennas (RHCP and LHCP) were helixes with 14-dB gain and 3-dB beamwidths of approximately 45 deg along both principal planes. These antennas were manually pointed toward the satellite at the beginning of each run, thus restricting data acquisition to straight road sections.

Receiver and Data Acquisition System

Measurements were made with a receiver/data acquisition system installed inside a passenger van operated by the University of Texas and shipped to Australia. The receiver had three outputs with two noise bandwidths. Recorded were in- and quadrature-phase detector voltages (noise bandwidth = 1 kHz) containing both amplitude and phase information for propagation analysis and later playback in hardware simulators. Also recorded was the output from a power detector with predetection bandwidth of 200 Hz. This bandwidth was chosen because it achieved a better signal-to-noise ratio (SNR) for shadowing measurements and, at the same time, enabled the reception of most Doppler-shifted multipath components when driving at highway speeds.

During the experiment, the receiver utilized an automatic frequency control circuit to keep the satellite line-of-sight signal in the center of the 200-Hz filter, thus eliminating frequency variations due to instrument drift and Doppler shift caused by satellite and vehicle motion. The maximum possible Doppler shift of multipath components due to scatterers straight ahead and behind the vehicle was ±130 Hz at the maximum vehicle speed of 25 m/s. For satellite illumination from the side, there was no Doppler shift of the direct signal, and a 260-Hz receiver bandwidth (depending upon the satellite elevation) would be required to receive all multipath components. If the satellite illumination were to emanate from the front or back, the direct signal would be shifted up or down by some 70–100 Hz, respectively. The Doppler shifted multipath components could, therefore, appear at maximum offsets of 230 Hz and 30 Hz relative to the direct wave. The narrow receiver filter eliminated some of the multipath signals and, because of the geometric linkage between signal direction and Doppler shift, effectively made the azimuth pattern of the low-gain antenna more directive.

Several factors combined to make the significant Doppler shifts less than the computed maximum. The low-gain antenna received scattered energy mainly from objects located within a cone centered above the car, which intersected with scatterers, such as trees or utility poles, mainly to the side of the vehicle, as 1) no stationary scatterers were straight ahead or behind on the road, 2) the low-gain antenna's gain drops off rapidly for elevation angles less than 15 deg, and 3) the influence of scatterers diminishes with increasing distance.[7] Comparisons of cumulative fade distributions derived from the quadrature signals and the 200-Hz channel gave very similar results, confirming this argument. The high-gain antenna was always pointed at the satellite and was less sensitive to multipath reception from directions away from its axis, again reducing the receiver bandwidth requirement.

The receiver system inside the van was connected through data acquisition equipment to a personal computer. The L-band data were sampled at a 1-kHz rate and stored on a magnetic disk in sequential records of 1024 samples. Vehicle speed and time were recorded only once per second.

The unfaded signal level was determined from the data itself. It was taken to be the average level of the signal observed while driving in a location that produced minimal multipath and no shadowing; all the data reported are relative to that level. ETS-V had unshadowed SNR values of approximately 22 dB (low-gain antenna) and 32 dB (high-gain antenna), IPORS had a SNR of 16 dB (low-gain antenna used only). In an effort to examine data uncorrupted by noise, only signal levels with an SNR margin greater than 7 dB were used in the analysis.

Road Features

The characteristics of roads over which attenuation data have been examined are summarized in Table 2. The column headings are defined as follows:

RUN# = an identifying number for a particular stretch of road and measurement configuration

DIST = the total road distance over which data were

obtained for this run, km
DIR = the azimuth direction to the satellite referenced to the vehicle direction, deg
ENV = the road environment characterized as follows: first letter (H = hilly, M = mountain, R = rolling), second letter (R = rural, S = suburban)
OBS = the type of roadside obstacles characterized as follows: T—trees, U—utility poles
SAT = satellite platform (ETS-V or IPORS)
GAIN = gain of receiving antenna (HIGH = high-gain, LOW = low-gain)
POL = polarization received (CO = copolarization, X = cross-polarization)
FADE(1%) = fade in dB exceeded at the 1% probability level

The vehicle heading, DIR, represents an average direction. The roads sampled generally have a number of twists and bends, resulting in variable local azimuths to the satellite. For roads having multiple type obstacles, such as both trees and utility poles, the categorization is also given in terms of which obstacles dominated. For example, TU implies the dominance of trees with a lesser number of utility poles alongside the road. Where the road types have multiple characteristics, such as rolling-rural or mountainous-rural, we specify these by RR and MR, respectively.

Measurements were made along suburban and rural roads in the Sydney area and southeastern Australia in noncontiguous blocks of about 30–70 km. Two major vegetation zones[10] were traversed in the experiment: forests along the coastal roads and woodlands (woodland and low-open woodland) further inland. Forests ranged from dry sclerophyll (most runs), in which the crowns of trees do not touch each other, to tropical rainforest (run 385), in which the leafy crowns of the trees intermingle. The dominating tree genus in the forests was Eucalyptus. The landscape, of course, has been modified by road construction. Other than tree types, more similarities than differences existed between apparent roadside conditions (tree heights, densities, setbacks) in Australia and the eastern United States.

Fade Distribution Results

Figures 1–4 show measured fade results. Attenuation levels are expressed in dB, relative to the unfaded reference power. Although only positive values of fades are shown in the graphs, negative values (signal enhancements) were also measured. Since they do not degrade the transmissions, they have not been plotted. The distributions are presented with the ordinate depicting the percentage of the distance over which the attenuation exceeded the abscissa (fade) level. As the speed was generally maintained constant over each of these runs, the ordinates also represent the percentage of time the abscissa

Table 2 Listing of runs with road types and characteristics

Run#	DIST, km	DIR, deg	ENV[a]	OBS[b]	SAT-GAIN-POL	FADE (1%), db
322*	6.6	315	RS	TU	ETS-LOW-CO	10.0
330	3.5	260	RR	UT	ETS-LOW-CO	6.7
331	4.8	80	RR	UT	ETS-LOW-CO	2.8
336*	41.9	275	MS	TU	ETS-LOW-CO	10.6
341*	3.5	45	RR	T	ETS-LOW-CO	10.7
342*	8.1	45	RS	TU	ETS-LOW-CO	13.2
343	2.4	265	RS	T	ETS-LOW-CO	>15.0
344	2.6	85	RS	T	ETS-LOW-CO	>15.0
354*	5.6	350	RR	T	ETS-LOW-CO	14.5
346	4.2	135	RR	T	ETS-LOW-CO	8.8
347*	5.2	315	RR	T	ETS-LOW-CO	13.1
348*	3.7	170	RR	T	ETS-LOW-CO	11.1
357	1.8	50	RS	UT	ETS-LOW-CO	2.6
359*	1.5	230	RS	TU	ETS-LOW-CO	10.2
362	1.6	230	RS	TU	ETS-LOW-CO	4.2
364	1.5	230	RS	UT	ETS-LOW-CO	6.4
365	1.7	140	RS	UT	IPO-LOW-CO	5.5
366	1.6	50	RS	UT	IPO-LOW-CO	2.1
367	1.7	320	RS	TU	IPO-LOW-CO	> 9.0
368	1.6	230	RS	UT	IPO-LOW-CO	3.1
369	1.7	50	RS	UT	IPO-LOW-CO	2.1
370	1.6	140	RS	TU	IPO-LOW-CO	> 9.0
371	1.6	230	RS	UT	IPO-LOW-CO	1.6
372	1.7	320	RS	UT	IPO-LOW-CO	8.5
377*	3.6	180	RR	T	ETS-LOW-CO	15.0
379*	49.8	325	HR	T	ETS-LOW-CO	10.9
380*	60.9	350	RR	T	ETS-LOW-CO	11.8
383*	33.0	330	HR	T	ETS-LOW-CO	13.1
385*	73.5	100	HR	T	ETS-LOW-CO	14.0
390*	56.0	265	HR	T	ETS-LOW-CO	12.5
391*	55.3	85	HR	T	ETS-LOW-CO	10.9
392	55.0	310	HR	T	IPO-LOW-CO	> 9.0
394	4.6	260	RR	UT	ETS-HIGH-CO	6.5
399	5.0	80	RR	UT	ETS-HIGH-CO	1.9
406	1.8	280	RS	UT	ETS-HIGH-CO	>15.0
408	1.7	280	RS	UT	ETS-HIGH-X	23.5
409	1.8	265	RS	T	ETS-HIGH-CO	24.2

[a] 1st letter: H = hilly, M = mountain, R = rolling; 2nd letter: R = rural, S = suburban.
[b] T = tree, U = utility pole, in order of relative frequency of occurence.

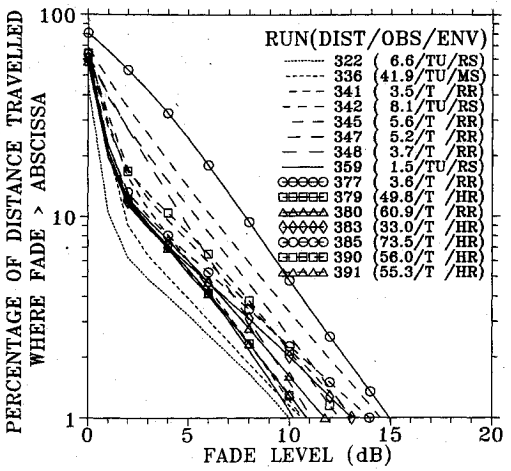

Fig. 1 Cumulative fade distribution functions for rural and suburban runs, with trees and/or utility poles causing shadowing of the signal from ETS-V.

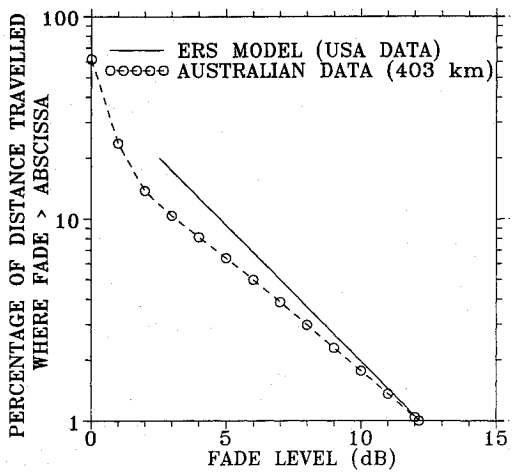

Fig. 2 Comparison of combined Australian tree runs with the empirical roadside shadowing model derived from U.S. data.

fade values were exceeded. The distributions show fade levels from 0 to 20 dB at 1-dB increments over the percentage range 1–100%. As mentioned previously, fades for the "low-gain mode" were calculated up to 15 dB, and those for the "high-gain mode" up to 25 dB, resulting in a 7-dB SNR at both limiting values.

Worst-Case Fade Levels

Figure 1 presents the fade distributions of individual runs marked with an asterisk in Table 2. These runs are characterized as follows: 1) they were made in rural or suburban areas, 2) they all show fades due to trees and utility poles of 10 dB or more at the 1% probability level, and 3) they represent measurements made with ETS-V in the low-gain mode. Excluded from this data set are two runs (343 and 344) along an approximate 2.5-km stretch of a suburban road lined on both sides with overhanging dense trees, where the vehicle passed through a virtual tunnel of vegetation, resulting in extreme shadowing. The distributions for these runs are presented in Figs. 3 and 4 and are described in a following section.

A quantitative physical interpretation relating the individual curves to specific measured roadside parameters is complex and has not been possible; the roads have varying densities of trees and utility poles along their sides with different setbacks, and also a variable local azimuth to the satellite due to bends in the roads. The worst-case distribution shown in Fig. 1 (run 377) has an average 45 deg azimuth direction. The road winds along a small river, and makes large local direction changes. The many trees along this narrow road have only minimal setbacks, and their branches frequently extend over the road. The smallest level fade distribution (run 322) has an azimuth of 315 deg, which is between the maximum and minimum shadowing geometry. The trees along this wide multilane road are not very close to its edge. We note that fades exceed values from 10 to 15 dB and 1 to 8 dB at the 1 and 10% probabilities, respectively.

Comparison with ERS Model

A model has been derived empirically from 640 km of measurements in central Maryland, employing both helicopter and the MARECS-B2 satellite transmitter platforms.[5] It represents the average fade statistics for various road types comprising predominantly tree and some utility pole roadside obstacles. It includes different sides of the roads driven, as well as different directions of travel relative to the line of sight propagation path.

The empirical roadside shadowing (ERS) model has the following form:

$$F = -M \cdot \ln(P) + B \qquad (\text{for } 20\% > P > 1\%) \tag{1}$$

where the slope is

$$M = 3.44 + 0.0975 \cdot \Theta - 0.002 \cdot \Theta^2 \tag{2}$$

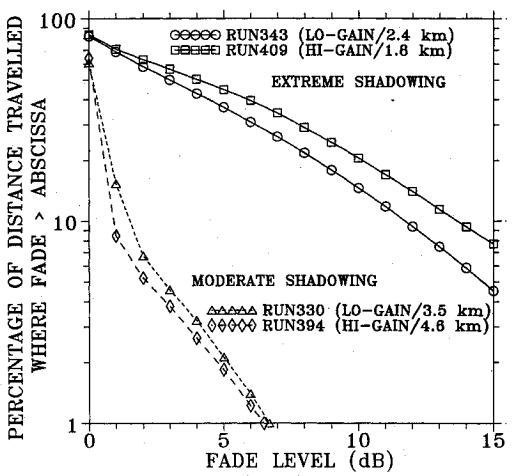

Fig. 3 Distributions of fades measured with a low- and a high-gain antenna for extreme and moderate shadowing conditions.

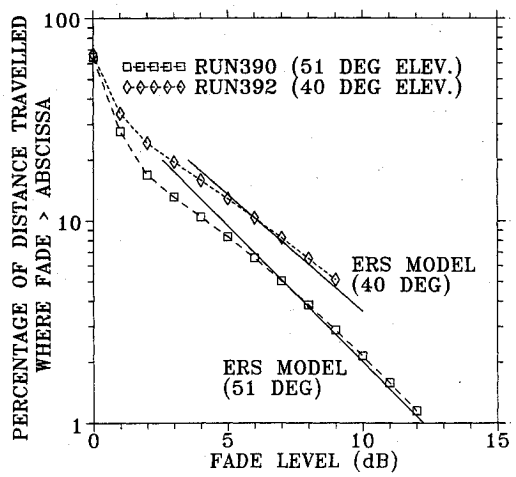

Fig. 4 Test of the empirical roadside shadowing model's elevation angle scaling against measured fade distributions for ETS-V and IPORS satellites at 40- and 51- deg elevation.

and the offset is

$$B = -0.443 \cdot \Theta + 34.76 \quad (3)$$

Figure 2 combines the fade histograms for the 15 individual runs of Fig. 1 into a single fade distribution (dashed line) comprising 403 km of roads. Also plotted (solid line) is the fade distribution, as predicted by the model. It is valid over the probability interval from 1% to 20%. We note that the maximum difference between the two distributions is less than 2 dB at the 14% probability level. The distribution depicted in Fig. 2 corresponds to $\Theta = 51$, and is given by

$$F = -3.21 \cdot \ln(P) + 12.2 \qquad (20\% > P > 1\%) \quad (4)$$

The closeness of the two results, although based on measurements made in different continents, represents a dramatic validation of the ERS model.

Distributions from Low- and High-Gain Receiving Antennas

During the campaign, nine repeated runs were implemented in which high- and low-gain receiver antennas were used for satellite measurements. The characteristics of these antennas are summarized in Table 1. Figure 3 shows typical high- and low-gain fade distributions. In the case of unusually heavy shadowing alluded to earlier, we note that the high-gain antenna experiences consistently deeper fading than the low-gain system. The fade differential increases from 0 dB at the median to approximately 3 dB at 4% of the distance traveled. We explain this slight increase in attenuation for the high-gain case as follows. The attenuations for both antenna cases are due to a combination of tree absorption of the direct energy and scattering of energy out of and into the antenna beam. When the beam is narrower, less power is received via the scattering mechanism. Conversely, the low-gain, azimuthally omni-directional antenna receives more scattered multipath contributions, and the averaged received power is enhanced. Whether this additional power has to be treated as noise or additional signal power depends upon its delay relative to the direct signal path. The high-gain antenna nevertheless, has 10 dB more gain, and the net power received by it is still significantly higher than that for the low-gain system (i.e., 7 dB more at 4% probability). This preserves the better SNR obtained with the high-gain antenna and its resulting systems performance advantage. The other pair of curves corresponds to a run that was shadowed only occasionally, with the fades caused by shadowing and multipath from isolated trees and utility poles. Insignificant fade differences existed between the low- and high-gain cases (i.e., less than 1 dB). Both of the cases demonstrate that the dominant cause of fading is shadowing along the line-of-sight, as opposed to multipath from ambient scatterers.

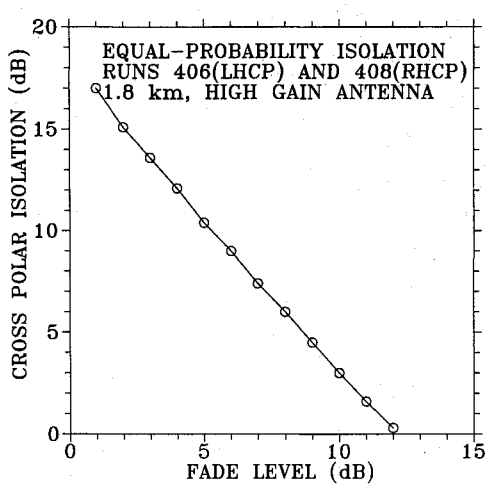

Fig. 5 The equal-probability polarization isolation for frequently shadowed conditions as a function of the copolar attenuation.

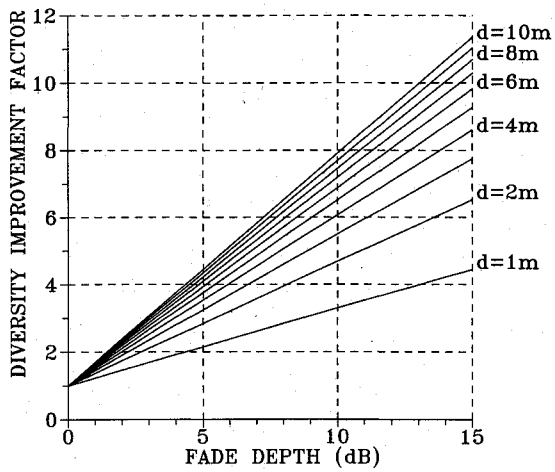

Fig. 6 An empirically derived family of curves of the DIF(F,d) as a function of fade depth F and for antenna separations d from 1 to 10 m.

Comparison of ETS-V and IPORS Measurements

Figure 4 compares repeated runs along the same road of measurements made with both the ETS-V and IPORS satellites. The fade levels for the IPORS measurements are observed to be always larger than those for ETS-V. The ERS model [Eqs. (1-3)] predicts that this result should occur because the elevation angle of IPORS (40 deg) is less than that for ETS-V (51 deg).

The IPORS fade is shown to exceed that of ETS-V at the 3% probability level by 2 dB. Figure 4 is based on data taken over a 55-km tree-lined road in the hills to the west of Sydney. This road was generally west-to-east, but made many turns following the contours of the landscape. Added to this figure are the median cumulative distribution functions predicted from the ERS model. For both satellites, the errors are less than 1 dB over the percentage range of validity (20%–1%). The elevation angle dependence is well represented by the model.

Co- and Cross-Polarization Measurements

Consecutive ETS-V measurements along a road shadowed by many trees were made with co- and cross-polarized high-gain antennas. Although these measurements were not made at the same time, we nevertheless may derive a statistical measure of the isolation at the different fade levels by defining the "equal-probability isolation" as the ratio of the cross-polarized to the copolarized signal levels at equal probability values. In Fig. 5, the equal-probability isolation corresponding to probabilities of 75%–3% are plotted as a function of the copolarization fade. We note that the isolation is 17 dB at the 1-dB fade level, and monotonically reduces to 0 dB at the 12-dB fade level. We may conclude from these results that frequency reuse systems employing dual polarizations from the same satellite are impractical because of poor isolation caused by multipath scattering into the cross-polarized channel. A discussion of the merit of frequency reuse with spatially separated satellites is beyond the scope of this paper.

Antenna Diversity Improvement

A convenient descriptor for characterizing the improvement in communications for a space diversity configuration is the diversity improvement factor (DIF) defined by

$$\mathrm{DIF}\,(F,d) P_0(F)/P_d(F) \quad (5)$$

where $P_0(F)$ represents the single terminal probability distribution at the fade depth F, and $P_d(F)$ represents the joint probability distribution for an antenna spacing d along the driving direction, assuming the same attenuation F is exceeded. We found, for instance, that DIF(8,1) is approximately 3,

which implies that, when the antennas are separated 1 m, the equivalent time over which the fade margin of 8 dB is exceeded is three times greater for the single terminal system as compared to diversity pair operation. Hence, assuming an 8-dB fade margin and a 6-min total "downtime" for the single terminal case, the outage for the diversity system would only be 2 min.

A least-square estimate of DIF was derived from the 403-km data base comprising Fig. 2 and found to be

$$\mathrm{DIF}(d,F) = 1 + [0.2 \cdot \ell_n(d) + 0.23] \cdot F \qquad (6)$$

In Fig. 6 are plotted a family of curves depicting DIF as a function of fade depth for antenna separations between 1 and 10 m. We note that with increasing separation for any given fade depth the rate of improvement of DIF diminishes.

Summary and Conclusions

The Australian campaign has provided an opportunity to validate a fade distribution model developed from U.S. measurements[5] with data obtained on a different continent. It has also made it possible to investigate new concepts hitherto not examined, namely, 1) the advantages of diversity operation, 2) the practicality of employing frequency reuse from mobile satellite systems, and 3) the effects of antenna directivity on fade distributions.

Specifically, the results demonstrate the following:

1) The fade statistics due to roadside trees and utility poles along rural or suburban roads in Australia are typical of those in the U.S., with similar densities of roadside obstacles.

2) The overall average fade distribution of 15 typical runs (Fig. 1), which exhibited fading of 10 dB or more at the 1% level, was found to agree with the fade distribution predicted by the ERS model[5] to within 2 dB over the probability level range of 1%–20% (Fig. 2).

3) Using an antenna with more gain under the severe shadowing condition resulted in more fading than was observed with a less directive antenna. For the example shown (Fig. 3), approximately 3 dB more attenuation at 4% probability resulted. The more directive pattern had about 45-deg beamwidths along the principal planes (14-dB gain), and the less directive system had an azimuthal omni-directional pattern, with a 60-deg beamwidth in elevation (4-dB gain). Although there is a fade increase for the more directive system, this is more than offset by the significant gain improvement for the system. The higher gain system also resulted in longer nonfade durations.

4) Comparison of fade distributions along the same section of roads employing the ETS-V and IPORS satellite transmitter platforms demonstrated deeper fades for the latter platform. These results are consistent with the fact that the IPORS elevation angle (40 deg) was significantly smaller than that for ETS-V (51 deg). Enhanced shadowing at the smaller elevation angles results in increased attenuation. The measured results were also found to be consistent with the ERS model (Fig. 4).

5) Frequency reuse by simultaneously transmitting opposite sense polarizations does not appear to be a viable option for Mobile Satellite Service communications, since depolarization due to obstacles in the vicinity of the line-of-sight reduces the isolation to unacceptable levels (Fig. 5).

6) A theoretical analysis suggests that unavailability can be reduced by a factor ranging from 2 to 8, if two antennas are employed in conjunction with a more elaborate receiver (Fig. 6). The degree of difficulty in achieving this improvement depends on the receiver implementation.

Acknowledgments

The authors are grateful to AUSSAT for sharing in the costs of this experiment and to AUSSAT's Mobilesat group for invaluable logistical and technical support during the campaign. Many thanks are also extended to the Japanese government for providing the satellite transmissions of ETS-V. We also acknowledge INTELSAT for enabling measurements with IPORS. G. W. Torrence of the Electrical Engineering Research Laboratory significantly participated in the development of the receiver system and the acquisition of the data. Y. Hase was supported by a grant from the Science and Technology Agency of Japan during his 1988–1989 stay at the University of Texas as a visiting researcher. This work was supported by the Jet Propulsion Laboratory for the University of Texas under Contract JPL956520, and by NASA Headquarters for the Applied Physics Laboratory of the Johns Hopkins University under Contract #N00039-89-C-5301.

References

[1]Vogel, W. J., and Goldhirsh, J., "Tree Attenuation at 869 MHz Derived from Remotely Piloted Aircraft Measurements," *IEEE Transactions on Antennas and Propagation,* Vol. AP-34, No. 12, 1986, pp. 1460–1464.

[2]Goldhirsh, J., and Vogel, W. J., "Roadside Tree Attenuation Measurements at UHF for Land-Mobile Satellite Systems," *IEEE Transactions on Antennas and Propagation,* Vol. AP-35, No. 5, 1987, pp. 589–596.

[3]Vogel, W. J., and Goldhirsh, J., "Fade Measurements at L-Band and UHF in Mountainous Terrain for Land Mobile Satellite Systems," *IEEE Transactions on Antennas and Propagation,* Vol. AP-36, No. 1, 1988, pp. 104–113.

[4]Goldhirsh, J., and Vogel, W. J., "Mobile Satellite System Fade Statistics for Shadowing and Multipath from Roadside Trees at UHF and L-Band," *IEEE Transactions on Antennas and Propagation,* Vol. AP-37, No. 4, 1989, pp. 489–498.

[5]Vogel, W. J., and Goldhirsh, J., "Mobile Satellite System Propagation Measurements at L-Band Using MARECS-B2," *IEEE Transactions on Antennas and Propagation,* Vol. AP-38, No. 2, 1990, pp. 259–264.

[6]Goldhirsh, J., and Vogel, W. J., "Propagation Degradation for Mobile Satellite Systems," *Applied Physics Lab. Technical Digest,* Vol. 9, No. 2, Johns Hopkins Univ., Baltimore, MD, April–June 1988, pp. 73–81.

[7]Vogel, W. J., and Hong, U. S., "Measurement and Modeling of Land Mobile Satellite Propagation at UHF and L-Band," *IEEE Transactions on Antennas and Propagation,* Vol. AP-36, No. 5, 1988, pp. 707–719.

[8]Butterworth, J. S., "Propagation Measurements for Land-Mobile Satellite Systems at 1542 MHz," Communications Research Centre, Ottawa, Canada, TN No. 723, Aug. 1984.

[9]Jongejans, A., Dissanayake, A., Hart, N., Haugli, H., Loisy, C., and Rogard, R., "PROSAT—Phase 1 Report," European Space Agency TR ESA STR-216, Paris, May 1986.

[10]Anon., *Think Trees Grow Trees,* Dept. of Arts, Heritage, and Environment, Australian Government Publishing Service, Canberra, Australia, 1985.

Alfred L. Vampola
Associate Editor